CRYSTAL GROWTH & DESIGN

Article

pubs.acs.org/crystal

Role of Brucite Dissolution in Calcium Carbonate Precipitation from Artificial and Natural Seawaters

Dan Nguyen Dang,*[,†] Stéphanie Gascoin,[‡] Alaric Zanibellato,[§] Cosmelina G. Da Silva,[†,‡] Mélanie Lemoine,[†] Benoît Riffault,[†] René Sabot,[§] Marc Jeannin,[§] Daniel Chateigner,[‡] and Otavio Gil[†]

[†]Normandie Université, UNICAEN, UNIROUEN, ABTE, 14000 Caen, France

[‡]Normandie Université, ENSICAEN, UNICAEN, CNRS, CRISMAT, 14000 Caen, France

[§]Université de La Rochelle, CNRS, LaSIE, 17000 La Rochelle, France

S *Supporting Information*

ABSTRACT: Brucite is often associated with calcium carbonate in calcareous scales. In this study, we focus on the effects of brucite dissolution on the carbonate precipitation. Brucite-saturated solutions are elaborated by adding the same amount of brucite powder in various volumes of different natural and artificial seawaters (natural organic materials are also added, with or without Mg^{2+} ions). The Mg^{2+} and Ca^{2+} concentrations in seawater at the beginning and end of the experiments are determined by ICP-AES. The solid powders are *ex-situ* analyzed using XRD and SEM. It is observed that brucite dissolution leads to pH increase and enrichment of seawaters in magnesium ions. The Mg^{2+} ions, either pre-existing in the solution or added from brucite dissolution play a key role in $CaCO_3$ polymorph selection. In order to separate the Mg^{2+} and OH^- effects, $CaCO_3$ precipitation is induced by NaOH addition in artificial seawater with or without Mg^{2+}. Under both NaOH and $Mg(OH)_2$ addition, only aragonite is precipitated from artificial and natural seawaters in our conditions. NaOH addition in Mg-free seawater allows us to predominantly obtain vaterite or calcite polymorphs, while both aragonite and calcite precipitates are observed from Mg-free seawater when NaOH is replaced by $Mg(OH)_2$. Natural organic materials added in artificial seawater have a significant effect on aragonite morphology.

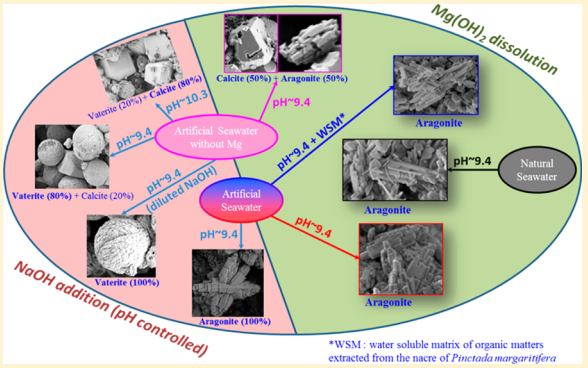

INTRODUCTION

Calcium carbonate plays a fundamental role in marine ecosystems. It is an important and usually one of the dominant minerals in marine sediments.[1] The mechanisms of $CaCO_3$ formation in both aqueous solution[2−12] and seawaters[1,13−22] have been studied by numerous authors. The rate of calcium carbonate formation in solution increases with temperature, which implies that its solubility decreases.[5] The most important calcium carbonate polymorphs in seawater are aragonite and calcite. Other phases (i.e., vaterite, hydrated $CaCO_3$) are far less abundant and of much lower importance, except for particular cases corresponding to biomineralization processes,[23] high ion concentrations, or the presence of microrganisms.[20] Seawater is supersaturated with respect to calcite and aragonite, and this supersaturation should favor a massive precipitation of calcium carbonate. However, calcium carbonate precipitation in surface seawater is almost absent. This has been explained by the presence of soluble organic matter (e.g., humic compounds) or dissolved phosphate interacting with the surface of crystals.[20,24,25] Berner et al.[25] suggested that the supersaturation of surface seawater with respect to aragonite is maintained because suspended particles, which may play a role as precipitation nuclei, are coated by humic compounds or dissolved phosphate. Magnesium plays a key role in calcite−aragonite polymorph selection. The role of magnesium in the crystal growth of calcite and aragonite from seawater has been studied for a long time.[1,17,20,21,26,27] Berner[26] concluded that dissolved magnesium in seawater has a strong retarding effect on calcite crystal growth rate but no effect on that of aragonite. The inhibition effect of Mg^{2+} on calcite growth rate is due to its incorporation within the crystal structure, resulting in the considerably more soluble magnesian calcite (Mg-calcite). However, a recent study of Sun and co-workers[21] shows that the increased solubility of Mg-calcite has negligible impact on nucleation rates, and the inhibition of calcite nucleation upon Mg^{2+} uptake is primarily due to an increase in surface energy.

A tremendous amount of work has been dedicated to the understanding of $CaCO_3$ biomineralization.[28,29] The mollusk shell is a product of biomineralization of $CaCO_3$ crystals. Nacre is a composite consisting of aragonite pseudohexagonal crystals embedded in an organic matrix.[30] This biomaterial is biocompatible and is known to have some osteogenic effect in

Received: September 1, 2016
Revised: February 11, 2017
Published: February 13, 2017

DOI: 10.1021/acs.cgd.6b01305
Cryst. Growth Des. 2017, 17, 1502−1513

sheep,[31] mouse,[32] rat,[33] and human[34] mammals. Rousseau et al.[30] have suggested that nacre water-soluble organic matrix (WSM) from the bivalve *Pinctada margaritifera* could speed up the differentiation and mineralization of damaged bone tissue. Although the organic matrix is quantitatively a minor constituent in the shell of mollusks (typically less than 5 wt %), it is however the major component that controls different aspects of the shell formation processes.[29]

In reality the $CaCO_3$ precipitation mechanism needs supersaturation conditions obtained by an increase of carbonate concentrations due to physicochemical displacements of acid−basic carbonic equilibrium in seawater. This phenomenon can particularly be induced by technological processes involving seawater electrolysis, in which calcium carbonate precipitation is always associated with that of brucite ($Mg(OH)_2$), forming a mineral scale called calcareous deposit. Brucite is also a thermodynamically stable product of serpentinization in hydrothermal vent systems.[35] The analysis of chimneys collected from the serpentinite-hosted Lost City hydrothermal field[36] and in the Southern Mariana Forearc[37] has indicated that it consists mostly of brucite and aragonite. Many studies of brucite surface chemistry have focused on its precipitation and dissolution kinetics.[38−41] Calcareous scales formed during the cathodic protection of metals in seawater are reported to consist of mainly $CaCO_3$ and $Mg(OH)_2$ (brucite). The $Mg(OH)_2/CaCO_3$ ratios in calcareous scales depend strongly on the applied potentials. Many studies[42−44] show that brucite is predominantly observed for more cathodic potentials, while less cathodic potentials favor $CaCO_3$ formation. Nevertheless, few studies exist on the effect of brucite dissolution on carbonate calcium precipitation from seawater.

The objective of this paper is to study the role of brucite dissolution in $CaCO_3$ precipitation from seawaters. The effect of WSM extracted from the nacre of *Pinctada margaritifera* on brucite dissolution and $CaCO_3$ precipitation, especially its morphology, is also mentioned. Finally, the vaterite−calcite−aragonite polymorph selection under pH monitoring is studied.

EXPERIMENTAL SECTION

Four different seawater solutions were prepared.

NSW. Natural seawater (pH ≈ 8) was taken at the marine station of Luc-sur-Mer (France) where it was pumped directly from the English Channel and decanted to remove large-particle sediments.

ASW. Artificial seawater was prepared on the basis of the six main compounds present in the D1141-98 standard.[45] The composition is NaCl, 0.42 mol dm^{-3}; Na_2SO_4, 2.88×10^{-2} mol dm^{-3}; $CaCl_2{\cdot}2H_2O$, 1.05×10^{-2} mol dm^{-3}; $MgCl_2{\cdot}6H_2O$, 5.46×10^{-2} mol dm^{-3}; KCl, 9.32×10^{-3} mol dm^{-3}; and $NaHCO_3$, 2.79×10^{-3} mol dm^{-3}. To avoid precipitation of $CaCO_3$ and $CaSO_4$ while combining the constituents of ASW, we prepared it in two separate containers. In the first container, we prepared a solution containing NaCl, Na_2SO_4, KCl, and $NaHCO_3$ salts, while in the other, the desired amounts of $CaCl_2{\cdot}2H_2O$ and $MgCl_2{\cdot}6H_2O$ were dissolved. After the salts in the two solutions were completely dissolved in pure water, they were carefully combined while stirring. The pH of the solutions was sometimes adjusted to ∼8 with a few drops of 0.1 M NaOH (to reach a similar pH to natural seawater of the English Channel).

ASW + WSM. Water-soluble organic matrix (WSM), extracted from the nacre of *Pinctada margaritifera* using a methodology described elsewhere,[46,47] was added to ASW in order to reach a concentration of 100 mg of WSM/dm^3 of ASW.

ASW − Mg^{2+}. ASW to which no magnesium salt was added was prepared. In this, the ionic strength deficiency was compensated by addition of an excess of NaCl. The composition is NaCl, 0.53 mol cm^{-3}; Na_2SO_4, 2.88×10^{-2} mol dm^{-3}; $CaCl_2{\cdot}2H_2O$, 1.05×10^{-2} mol dm^{-3}; KCl, 9.32×10^{-3} mol dm^{-3}; and $NaHCO_3$, 2.79×10^{-3} mol dm^{-3}.

Precipitation Experiments. The experiments were carried out by adding the same amount (1 g) of brucite powder (Alfa Aesar 95−100.5%) in different volumes (50, 200, 500, and 900 cm^3) of the four seawaters. This brucite amount generates in any case brucite-saturated solutions at equilibrium conditions. The chemical speciation of the solutions was determined using the PHREEQC computer program.[48] More details of speciation calculations can be found in the Supporting Information.

In order to determine Mg^{2+} and Ca^{2+} concentrations, the solutions were analyzed by ICP-AES (inductively coupled plasma-atomic emission spectrometry, Varian, Vista MPX) at the beginning and at the end of the experiments. The evolution of Mg^{2+} and Ca^{2+} concentrations in aqueous phase permitted determination of the quantities of dissolved $Mg(OH)_2$, $m_{\text{diss-Mg(OH)}_2}$, and precipitated $CaCO_3$, $m_{\text{prec-CaCO}_3}$.

$$m_{\text{diss-Mg(OH)}_2} = ([Mg^{2+}]_f - [Mg^{2+}]_0)VM_{Mg(OH)_2} \quad (1)$$

$$m_{\text{prec-CaCO}_3} = ([Ca^{2+}]_0 - [Ca^{2+}]_f)VM_{CaCO_3} \quad (2)$$

where $[Mg^{2+}]_f$ and $[Ca^{2+}]_f$ are the Mg^{2+} and Ca^{2+} concentrations at the end of the experiments, $[Mg^{2+}]_0$ and $[Ca^{2+}]_0$ are the Mg^{2+} and Ca^{2+} concentrations at the beginning of the experiments, V is the seawater volume, and $M_{Mg(OH)_2}$ and M_{CaCO_3} are the molar masses of $Mg(OH)_2$ and $CaCO_3$.

The total solid mass variation at the end of the experiment, Δm, was calculated using the following formula:

$$\Delta m = m_{\text{prec-CaCO}_3} - m_{\text{diss-Mg(OH)}_2} \quad (3)$$

In order to understand the roles of pH and Mg^{2+} concentration on $CaCO_3$ precipitation from seawaters, other experiments were also carried out by gradually adding a NaOH solution in 900 mL of ASW or ASW − Mg^{2+} solutions to reach a pH of 9.4 or 10.3, respectively. These pH values have been chosen based on the values obtained at the end of the experiments of brucite dissolution in the seawaters.

The pH was measured with a Cyberscan pH510 from Eutech Instruments. Low, continuous solution agitation was maintained using magnetic stirring. All experiments were carried out at ambient temperature (20 ± 1 °C) and were performed in an open reactor during 24 h for the volumes 20, 200, and 500 cm^3 and 72 h for the 900 cm^3 solution.

Precipitated powders obtained at the end of these experiments were filtered, washed with ultrapure water to remove the soluble salts (in particular NaCl), and dried before X-ray diffraction (XRD) and scanning electron microscopy (SEM, Carl Zeiss 5500 instrument) experiments. X-ray powder diffraction data were collected using a D8 Advance Vario 1 Bruker two-circle diffractometer ($\theta-2\theta$ Bragg−Brentano mode) using the monochromatized Cu Kα radiation (λ = 1.540598 Å) and the Lynx Eye detector. Data were collected over the angular range $5° \le 2\theta \le 120°$ at room temperature counting for 0.8 s at each angular increment of 0.0105° (10 h/scan). XRD patterns analyzed using the combined analysis methodology[49] allow the quantitative determination of phase fractions.

RESULTS AND DISCUSSION

pH Evolution. In a preliminary test, brucite powder is added to stirred ultrapure water. The test is operated in a closed reactor to avoid $CO_{2(g)}$ dissolution and $MgCO_3$ or relevant phase precipitation. The pH increases abruptly to 10.3 ± 0.1 in just a few minutes and remains stable for the total duration of experiments. This pH is similar to the value numerically determined using the PHREEQC computer program (Table S1 of the Supporting Information). The pH increase is due to the brucite solubility (solubility product $pK°_{sp}$ = 10.5 ± 0.2 at 25 °C) and relatively fast dissolution kinetics:[40]

$$Mg(OH)_2 \rightleftharpoons Mg^{2+} + 2OH^- \quad (r1)$$

DOI: 10.1021/acs.cgd.6b01305
Cryst. Growth Des. 2017, 17, 1502−1513

Dissolution of the brucite powder in NSW, ASW, and ASW + WSM solutions (initial pH ≈ 8) results in a rapid increase in pH to 9.4 ± 0.1 after a few minutes. These pH values remain almost stable until the end of the tests (24 h for V = 50, 200, and 500 cm^3 and 72 h for V = 900 cm^3). Figure 1 shows the final pH values

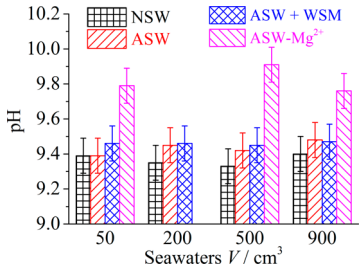

Figure 1. pH values in different seawaters at the end of brucite dissolution experiments (24 h for V = 50, 200, and 500 cm^3 and 72 h for V = 900 cm^3). NSW, natural seawater; ASW, artificial seawater; ASW + WSM, artificial seawater with WSM added; ASW − Mg^{2+}, artificial seawater without Mg^{2+}.

obtained at the end of the experiments. These measured pH values are consistent with the values simulated using PHREEQC (Table S1 and Figure S1 of the Supporting Information). A slight pH difference is observed among different volumes for the same seawater or among different seawaters but smaller than the measured pH standard deviation (±0.1). The difference between the pH obtained in the ultrapure water (~10.3) and seawaters (~9.4) can be partially explained by the pre-existence of Mg^{2+} ions in seawaters (~1300 $mg{\cdot}cm^{-3}$), which reduced the OH^- concentration according to the displacement of brucite dissolution equilibrium (reaction r1).

This remark is consistent with the pH ≈ 10.3 experimentally reached in the ASW − Mg^{2+} solution during the first 6 h. This value is similar to that obtained for the case of brucite dissolution in ultrapure water. Indeed, the absence of Mg^{2+} ions favors the equilibrium displacement in the direction of the dissolution and thus to a higher release of OH^-. However, after 6h of experiment, the pH begins to decrease slightly and reaches ~9.8 at the end of the tests. This pH decrease (that is not previously observed in ultrapure water) suggests that the buffer effect of seawater also played an important role. The reaction rate between HCO_3^- and CO_3^{2-} in the ASW − Mg^{2+} solutions (reaction r2), which is slower than that of brucite dissolution, leads to a slight and progressive decrease of pH and reaches ~9.8 at the end of the tests. Dreybrodt et al.[50] have found that the precipitation kinetics of calcite is controlled by the slow kinetics of the overall reaction $CO_2 + H_2O \rightleftharpoons HCO_3^- + H^+$. PHREEQC modeling of brucite dissolution equilibrium indicates that the pH obtained in ASW − Mg^{2+} solution (10.13) is slightly lower than the one reached in pure water (10.37). This difference confirms the role of the HCO_3^-/CO_3^{2-} equilibrium in the ASW − Mg^{2+} solution.

$$HCO_3^- + OH^- \rightleftharpoons CO_3^{2-} + H_2O \quad \text{(r2)}$$

$$Ca^{2+} + CO_3^{2-} \rightleftharpoons CaCO_3 \quad \text{(r3)}$$

Thus, the higher pH in ASW − Mg^{2+} solutions allows us to suggest that the amount of brucite dissolved in this solution is more important than that in other seawaters. Mass evolution (calculated form ICP-AES) and XRD results hereafter will allow validation of this hypothesis.

Mass Evolution. The quantities of dissolved brucite and precipitated calcium carbonate and the total mass variation, Δm, are determined based on the ICP-AES analysis (Figure 2).

It can be seen that Δm evolves (Figure 2a) roughly linearly with the initial volume of seawaters and is coherent with the final pH values (Figure 1). The increase of experiment time from 24 to 72 h seems to have minor effect on the solid mass evolution. These Δm variations result from the competition between brucite dissolution (Figure 2b) and calcium carbonate precipitation induced by the pH change (Figure 2c). It is important to note that only $Mg(OH)_2$ and $CaCO_3$ (calcite and aragonite polymorphs) are found by SEM and XRD analysis (detailed in next section), other numerically supersaturated phases (e.g., magnesite, dolomite, or relevant phases, Table S1 and Figure S1) are not experimentally detected. Figure 2b indicates that $m_{diss\text{-}Mg(OH)_2}$ is similar in natural and artificial seawaters with or

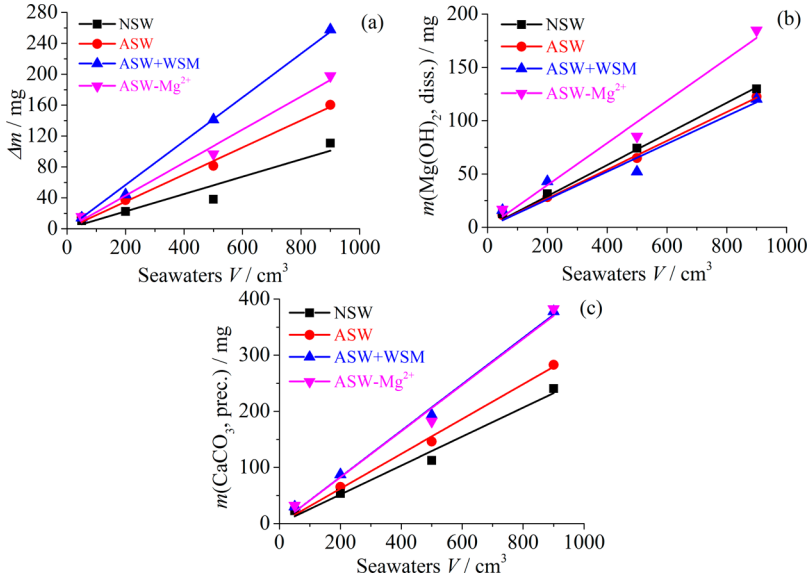

Figure 2. Evolution of (a) solid mass variation, Δm, (b) mass of dissolved $Mg(OH)_2$, and (c) mass of precipitated $CaCO_3$ as a function of initial seawater volumes.

DOI: 10.1021/acs.cgd.6b01305
Cryst. Growth Des. 2017, 17, 1502−1513

without WSM from *Pinctada margaritifera*. This nacre's WSM contains mainly two amino acids, glycine (42.5 wt %) and alanine (21.4 wt %), and HCO_3^- (20 wt %).[47] The amino groups of amino acids (glycine pK_{a2} 9.87; alanine pK_{a2} 9.78[51]) and bicarbonate ions might participate to buffer effects in seawater and seem to modify the amount of dissolved brucite (Figure 2b) and the final pH (Figure 1). However, this study is not detailed enough to conclude on the effects of this specific WSM on brucite dissolution. The amount of brucite dissolved via reaction r1 depends strongly on the pre-existing Mg^{2+} ions. The lower the pre-existing Mg^{2+} ions present, the higher the brucite dissolved (Figure 2b). Thus, the highest $m_{diss\text{-}Mg(OH)_2}$ and the highest pH are observed in ASW − Mg^{2+} solutions (Figure 1). The initial Mg^{2+} concentration, before adding brucite, in NSW (ICP-AES, 1287 mg·cm^{-3}) is slightly lower than that in ASW (ICP-AES, 1335 mg·cm^{-3}). Therefore, the quantity of dissolved brucite is slightly larger in NSW compared to ASW (with or without WSM). On the other hand, the WSM added in ASW significantly affects the $CaCO_3$ precipitation (Figure 2c): $(m_{prec\text{-}CaCO_3})_{ASW+WSM} > (m_{prec\text{-}CaCO_3})_{ASW}$. The larger amount of precipitated $CaCO_3$ in the ASW + WSM solution might be partially explained by the presence of HCO_3^- in WSM (about 20 wt %[47]). The WSM addition leads to a weak increase of $[HCO_3^-]$ in the ASW + WSM solution. Therefore, Δm exhibits its largest values in the ASW + WSM solutions (Figure 2a). The lowest Δm obtained from NSW is the result of the smallest amount of $CaCO_3$ precipitated because of the presence of soluble organic matter (i.e., humic compounds) and phosphate.[20,24,25] The lack of these organic matters in the artificial seawaters might be the origin of the larger amount of precipitated $CaCO_3$ (Figure 2c) and Δm (Figure 2a) in these solutions. We also see in Figure 2c that $CaCO_3$ precipitation is the largest in the ASW − Mg^{2+} (and in ASW + WSM) solution. The amount of $CaCO_3$ precipitated in ASW − Mg^{2+} (without Mg^{2+}) is larger than that obtained in ASW (with Mg^{2+}). This result suggests that the pH of the solution (controlled by brucite dissolution) has a significant effect on the rate of $CaCO_3$ precipitation (r3). So, the Δm obtained from ASW − Mg^{2+} (without magnesium ions) is larger than that from the ASW solution (containing Mg^{2+}). Many studies have focused on the role of magnesium ions on $CaCO_3$ crystal growth in seawaters.[1,17,26,52] Berner[26] has found that magnesium ions at seawater concentration levels appear to have no effect on the rate of crystal growth of aragonite but a strong retarding effect on that of calcite. In agreement with many previous results from literature, it can be observed from XRD and SEM analysis hereafter that both calcite and aragonite polymorphs precipitate after brucite dissolution in ASW − Mg^{2+} solution in which no Mg ions pre-existed.

In this study, the excessive amount of brucite powder has been chosen hoping that Ca^{2+} in the seawaters could totally react to form solid $CaCO_3$. Then, we assume that $m_{CaCO_3}^{calcd\text{-}Ca^{2+}} = n_{Ca^{2+}} M_{CaCO_3}$, where $n_{Ca^{2+}}$ is the number of moles of Ca^{2+} ions present in the seawaters. However, the number of moles of HCO_3^- ion, $n_{HCO_3^-}$ in seawaters is lower than that of Ca^{2+} and the amount of precipitated $CaCO_3$ should be controlled by the initial HCO_3^- concentration (with the assumption that HCO_3^- is the main carbonate form present in the seawaters). Consequently $m_{CaCO_3}^{calcd\text{-}HCO_3^-} = n_{HCO_3^-} M_{CaCO_3}$. Figure 3 shows a comparison between experimental mass, $m_{CaCO_3}^{exptl}$, and the maximum amount, $m_{CaCO_3}^{calcd\text{-}Ca^{2+}}$, calculated from the initial $[Ca^{2+}]$ concentration or the $m_{CaCO_3}^{calcd\text{-}HCO_3^-}$ calculated from the initial $[HCO_3^-]$ concentration in the seawaters.

It can be seen that the amounts of precipitated $CaCO_3$ are partially controlled by $[HCO_3^-]$ in the seawaters: $m_{CaCO_3}^{calcd\text{-}HCO_3^-} \leq m_{CaCO_3}^{exptl} \ll m_{CaCO_3}^{calcd\text{-}Ca^{2+}}$. Furthermore, $m_{CaCO_3}^{exptl}$ precipitated in ASW + WSM (Figure 3c) and ASW − Mg^{2+} (Figure 3d) are slightly larger than those calculated from HCO_3^- content of seawaters (and of WSM). This phenomenon is also found in ASW and NSW solutions (Figure 3a,b) when the lowest seawater volumes are used (i.e., 50 or 200 cm^{-3}). These results suggest that the increase of seawater pH due to brucite dissolution facilitates atmospheric $CO_{2(g)}$ absorption into the seawaters via the following equilibria:

$$CO_{2(g)} \rightleftharpoons CO_{2(aq)} \qquad \text{(r4)}$$

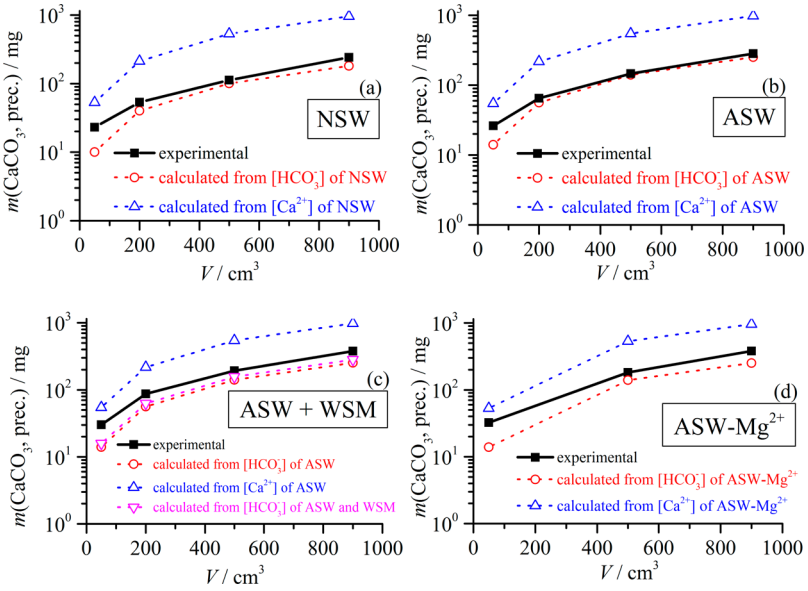

Figure 3. Evolution of experimentally precipitated mass of $CaCO_3$, $m_{CaCO_3}^{exptl}$, of calculated mass, $m_{CaCO_3}^{calcd\text{-}HCO_3^-}$ and $m_{CaCO_3}^{calcd\text{-}Ca^{2+}}$, as a function of initial seawater volumes: (a) NSW; (b) ASW; (c) ASW + WSM; (d) ASW − Mg^{2+} (logarithmic scale graphs).

DOI: 10.1021/acs.cgd.6b01305
Cryst. Growth Des. 2017, 17, 1502−1513

$$CO_{2(aq)} + 2H_2O \rightleftharpoons HCO_3^- + H_3O^+ \quad (r5)$$

$$H_3O^+ + 2OH^- \rightleftharpoons 2H_2O \quad (r6)$$

Then, the equilibrium displacement from $CO_{2(g)}$ to CO_3^{2-} allows an increase in $CaCO_3$ amount. Brucite dissolution in the seawaters favors $CaCO_3$ formation and can be imagined as a complementary ecological option for carbon dioxide sequestration, for instance, in artificial carbonate reef formations. Of course, further studies should be carried out before this aspect may be applied.

$CaCO_3$ Polymorphs after $Mg(OH)_2$ Dissolution. Results obtained from ICP-AES show that the Mg/Ca molar ratios are initially around 5 for the NSW, ASW, and ASW + WSM solutions (Figure 4). The brucite dissolution and calcium carbonate

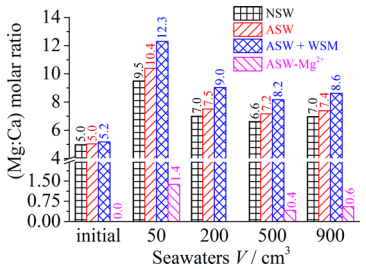

Figure 4. Mg/Ca molar ratios in the different seawater solutions at the beginning (before adding brucite) and at the end of the brucite dissolution experiments (24 h for V = 50, 200, and 500 cm^3 and 72 h for V = 900 cm^3).

precipitation lead to strong increases of Mg/Ca ratios. XRD patterns of the powders obtained after brucite dissolution in the different seawaters are shown in Figure 5. They indicate that the

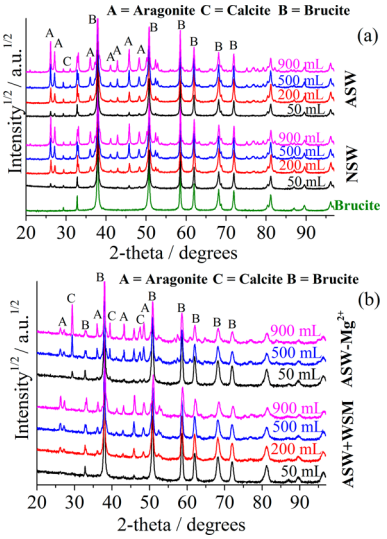

Figure 5. XRD powder patterns of brucite and powders obtained from NSW and ASW solutions (a) and ASW + WSM and ASW − Mg^{2+} solutions (b) at the end of the brucite dissolution experiments. A = aragonite; C = calcite; B = brucite.

aragonite polymorph is predominantly precipitated in the NSW, ASW, and ASW + WSM solutions in which the initial Mg^{2+} concentration is large. The brucite phase is not totally dissolved and is also found in the powders at the end of the experiments. PHREEQC modeling of brucite dissolution in the seawaters (Table S1 and Figure S1) shows that the solutions should be supersaturated with respect to magnesite and dolomite, upon equilibration with brucite. Magnesite is not expected to form at low temperature due to a kinetic inhibition related to the strong hydration of Mg^{2+} ions,[53] although it is the thermodynamically most stable Mg-carbonate.[54] This stable crystalline form may be found only under high temperature synthesis conditions either by reaction between MgO and CO_2 or by hydrothermal methods.[55] Dolomite formation from seawater is also little seen at low temperatures in the laboratory despite its extensive supersaturation.[1] The brucite and $CaCO_3$ polymorph weight percent have been quantitatively determined by treating the X-ray patterns within the Rietveld-based software MAUD[56] and are represented in Figure 6 (only wt % of aragonite and

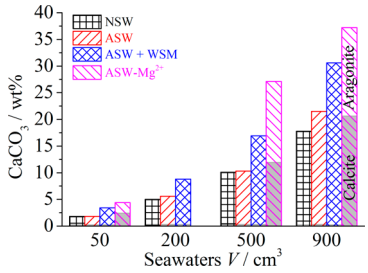

Figure 6. Evolution of $CaCO_3$ wt % in the solid powders obtained at the end of brucite dissolution experiements as a function of initial seawater volumes (aragonite, open bars; calcite, gray-filled bars; brucite, complement to 100 wt %.

calcite are present in Figure 6; the rest is brucite). We observe that in the NSW, ASW, and ASW + WSM solutions where the Mg^{2+} ions pre-existed, the brucite dissolution favors aragonite precipitation, while calcite is only present at very small ratio, typically lower than few percent. This explains why the calcite peaks are very small (Figure 5). Larger seawater volumes give rise to larger solid $CaCO_3$ wt % (mainly presented in aragonite polymorph) at the end of the experiments. We observe in Figure 4 that, for all seawaters containing Mg^{2+}, the Mg/Ca ratios are the largest (>9.5) for smallest seawater volumes (50 cm^3), consistent with the amount of precipitated $CaCO_3$ (Figure 3). This result suggests that the $CO_{2(g)}$ absorption rate into the seawaters is the largest, and consequently also the precipitation rate of $CaCO_3$, when seawater volumes are small (the same brucite powder mass is used for all seawater volumes). We also remark that Mg/Ca ratios are the largest in artificial seawater containing WSM. It might be partially explained by the presence of HCO_3^- in WSM (about 20 wt % of WSM[47]) but also by the role of WSM (seeds) in accelerating the $CaCO_3$ precipitation or $CO_{2(g)}$ absorption.

These large Mg/Ca ratios favor the formation of aragonite at the expense of calcite (Figures 5 and 6). This result is consistent with previous studies in the literature, concluding that the Mg/Ca molar ratio is the principal parameter governing the aragonite/calcite polymorph selection.[1,17,20,21] The combined effect of Mg^{2+} and SO_4^{2-} on the inhibition of calcite growth has also been studied by several authors. Mucci et al.[14] concluded that calcite growth rate in artificial seawater is lower than that in artificial seawater without SO_4^{2-}. A recent study by Nielsen et al.[57] reported that SO_4^{2-} is a much weaker inhibitor in comparison with Mg^{2+}, adsorbing on calcite surface and blocking growth sites. Mg^{2+} adsorbs and is incorporated into the growing calcite. Furthermore, the effect of Mg^{2+} is enhanced in the

DOI: 10.1021/acs.cgd.6b01305
Cryst. Growth Des. 2017, 17, 1502−1513

presence of SO_4^{2-} ions. Therefore, these ions inhibit calcite growth with magnitudes $SO_4^{2-} \ll Mg^{2+} < MgSO_4$. Sun et al.[21] have numerically predicted that using Mg/Ca seawater ratios around 5, aragonite nucleates up to 10 orders of magnitude more frequently than calcite. The inhibition of calcite nucleation upon Mg^{2+} uptake is primarily due to an increase in surface energy of its crystals, from 0.21 J/m^2 for pure calcite to 0.35 J/m^2 at the equilibrium of Mg(7%)-calcite, this latter surface energy being larger than that of aragonite (0.28 J/m^2) in seawater. Therefore, the surface energy favors a kinetic preference for aragonite nucleation in such conditions. However, aragonite does not accept Mg^{2+} incorporation into its structure at any Mg/Ca ratio, because of a much too large enthalpy of Mg-aragonite formation. Many studies cited in the review paper of Morse et al.[1] have observed that Mg/Ca ≈ 2 sets an effective boundary for polymorph selection between aragonite and magnesian-calcite, whereas a Mg/Ca > 2 promotes aragonite. This empirical observation was also successfully confirmed by numerical prediction.[21] Falini et al.[20] studied the role of Mg^{2+} ions on the precipitation of $CaCO_3$ phases by adding Mg^{2+} ions in the mixture of two solutions of $CaCl_2$ and Na_2CO_3 for 5 days and found that the presence at low concentration of Mg^{2+} ions, Mg/Ca = 1 or 2, promoted the precipitation of magnesian-calcite; aragonite and magnesian-calcite were precipitated with Mg/Ca = 3; aragonite, magnesian-calcite, and monohydrocalcite precipitated with Mg/Ca = 5; the precipitation of monohydrocalcite and aragonite only was detected with Mg/Ca = 7. In our study, the Mg/Ca ratio is also found around 7 or larger at the end of the experiments for all Mg^{2+}-seawaters. However, only pure aragonite with no trace of monohydrocalcite is observed in our case using ex-situ XRD and SEM analyses. This is not peculiarly astonishing for ex-situ observations since monohydrocalcite is known to be metastable with respect to calcite and aragonite and transforms to aragonite with time.[58] The formation of monohydrocalcite or relevant metastable phases might be monitored by in situ methods (e.g., IR or Raman spectroscopies) in future studies.

In artificial seawater without Mg^{2+} (ASW − Mg^{2+}), the Mg/Ca ratio at the end of the experiment is lower than 2 (Figure 4), and X-ray diffraction (Figure 5) shows that both Mg-calcite and aragonite are found in the final powders. The Mg-calcite/aragonite ratios are about 50:50 (Figure 6), increasing for larger solution volumes. At the first times upon incorporation of brucite into the solution, the local Mg/Ca ratio is not homogeneously distributed, resulting in calcite precipitation at Mg^{2+}-deficient locations in the volume and aragonite precipitation elsewhere. After homogenization, the remaining Ca^{2+} ions serve aragonite precipitation, as in our usual seawater conditions. Consequently, at larger solution volumes (900 cm^3) and for a fixed brucite amount (1 g) added to the solution, the relative calcite ratio in the precipitate increases. We hypothesize that the local Mg/Ca ratio on nucleation sites is controlled by ion diffusion transport[54] and might be quite different from the average ratio of the bulk solution. This local ratio varies with dissolving brucite and $CaCO_3$ precipitation. Hövelmann et al.[54] suggested that the carbonation reaction is locally diffusion-transport controlled and the carbonation nucleation predominantly occurred in areas of high brucite dissolution. The local Mg/Ca ratio might be initially lower and favors magnesian-calcite nucleation and growth. Then, this ratio increases with the increase of Mg^{2+} by brucite dissolution and the decrease of Ca^{2+} by calcium carbonate precipitation (to a level larger than the average value of the bulk solution), resulting in aragonite formation. Moreover, the amount of precipitated $CaCO_3$ polymorphs in the ASW − Mg^{2+} is larger than those in the natural and artificial seawaters with pre-existing Mg^{2+} ions. XRD results are coherent with pH values (Figure 1), solid mass variations (Figure 2), and Mg/Ca ratios (Figure 4).

Cell parameters refined from combined analysis of precipitated aragonite polymorph are shown in Table 1. They exhibit

Table 1. Combined Analysis Results for Aragonite Precipitated after Brucite Dissolution in Seawaters (900 cm^3)[a]

	ASW − Mg^{2+}	ASW	ASW + WSM	NSW
a (Å)	4.9618(3)	4.9631(1)	4.9632(1)	4.9651(1)
b (Å)	7.9678(5)	7.9706(3)	7.9714(3)	7.9737(3)
c (Å)	5.7473(3)	5.7465(2)	5.7470(2)	5.7497(2)
$\Delta a/a$	-0.06×10^{-4}	2.56×10^{-4}	2.76×10^{-4}	6.59×10^{-4}
$\Delta b/b$	-1.68×10^{-4}	1.83×10^{-4}	2.84×10^{-4}	5.72×10^{-4}
$\Delta c/c$	7.75×10^{-4}	6.36×10^{-4}	7.23×10^{-4}	1.19×10^{-3}
Ca y	0.4159(6)	0.4141(2)	0.4145(2)	0.4138(3)
z	0.7550(9)	0.7583(4)	0.7577(4)	0.7582(4)
C y	0.775(3)	0.772(1)	0.766(1)	0.773(1)
z	−0.084(4)	−0.083(2)	−0.087(2)	−0.081(2)
O1 y	0.922(2)	0.9233(8)	0.9226(8)	0.9235(9)
z	−0.093(2)	−0.0902(8)	−0.0929(8)	−0.0883(8)
O2 x	0.485(2)	0.4730(8)	0.4754(8)	0.4713(9)
y	0.685(1)	0.6814(5)	0.6819(5)	0.6815(6)
z	−0.095(2)	−0.0951(7)	−0.0931(8)	−0.0943(7)
Δz_{C-O1}, Å	0.009	0.007	0.006	0.007
GoF (%)	2.68	2.52	2.40	2.49
R_w (%)	10.13	9.10	8.93	8.90
R_B (%)	7.81	7.08	6.86	6.98
R_{exp} (%)	3.77	3.62	3.72	3.57

[a]Parentheses are standard deviations on the last digit. Reliability factors from combined analysis: GoF, goodness-of-fit; R_w, weighted factor; R_B, Bragg factor; R_{exp}, expected factor; a, b, c, unit-cell parameters of the crystals; x, y, z, atomic fraction coordinates; $\Delta z_{C-O1} = z$ coordinate of C−z coordinate of O1. Unit-cell parameters and atomic coordinate references for the non-biogenic aragonite are from Caspi et al.[59]

DOI: 10.1021/acs.cgd.6b01305
Cryst. Growth Des. 2017, 17, 1502−1513

cell distortions (a, b, c) compared to nonbiogenic aragonite determined by Caspi et al.[59] Such distortions exhibit slight anisotropy with the highest values in NSW and the lowest in ASW − Mg^{2+}. Similar cell expansions are found in the artificial seawater with and without addition of WSM. No large modifications of cell parameters as observed in the literature on similar works and no large SEM grains shape modifications also observed by some authors could be observed by adding WSM in the ASW solution. The slight modifications of grain shapes when comparing ASW and ASW + WSM of our studies only pokes for a tendency to resemble NSW-like conditions, which overall might be attributed to many components present in NSW other than WSM, as well as WSM itself. Consequently, WSM addition in ASW has no or minor effect on the cell parameters of aragonite. Only in the ASW − Mg^{2+} solution, the cell parameter contraction, in the a,b plane of aragonite, is found. However, these distortions are very low for all used seawaters if we compare with the cell parameters of biogenic aragonite of some mollusk shell species reported in the literature.[60,61] The combined analysis of precipitated aragonite polymorph indicates that in NSW, the mean coherent domains (crystallites) of aragonite adopt a roughly cylindrical shape, 62 nm in height and 38 nm diameter, with the cylinder axis aligned with the c-axis of the crystal structure, while in ASW, the long axis of the mean crystallites drops down to 55 nm. Such shapes and sizes are not significantly modified under WSM addition in the solution, while long crystallites develop along the [011] directions up to 170 nm in the absence of any Mg^{2+} cation in the initial solution. These microstructural observations again tend to reveal that WSM has only minor effects on the crystallinity of the precipitates, if any. Indeed if NSW, which always contains some parts of WSM due to dissolved bioorganisms, seems to favor slightly larger crystallites, addition of WSM in ASW shows slight but opposite behavior. WSM addition consequently seems to have very weak effects on both structural and microstructural characteristics of the crystals. Removal of initial Mg^{2+} cations tends to result in aragonite grains with larger coherent domain sizes. This might point toward a detrimental effect of Mg^{2+} also on aragonite and would merit further analysis but is beyond the scope of this work.

Figure 7 shows typical SEM images of precipitated calcium carbonate polymorphs obtained from different seawaters (with V = 900 cm^3). Aragonite appears as aggregates formed by small needle-like crystals for all seawaters. Although XRD reveals less aragonite size and shape modification for crystals obtained from different seawaters, SEM images indicate that aragonite grain shapes and sizes depend strongly on the kind of seawater. The needle-like aragonite crystals are very thin and long in the NSW (Figure 7a) but thicker and shorter in the ASW (Figure 7b). WSM addition in ASW modifies the morphology of precipitated aragonite, such that needle-like aragonite crystals in ASW + WSM (Figure 7c) become similar to those in NSW. In the literature, the effect of WSM extracted from the nacre of the oyster *Pinctada maxima* on the electrodeposited aragonite structure has been previously studied by Krauss.[62] This author found a significant decrease of the needle-like aragonite crystal sizes with WSM addition. The effect of adding the proteins isolated from individual genera *Rhynchonelliformea* was tested on $CaCO_3$ precipitation experiments, producing spectacular results in crystal morphology changes.[28] In mollusk shells containing nacre layers, nacre's WSM plays an important role in the macroscopic

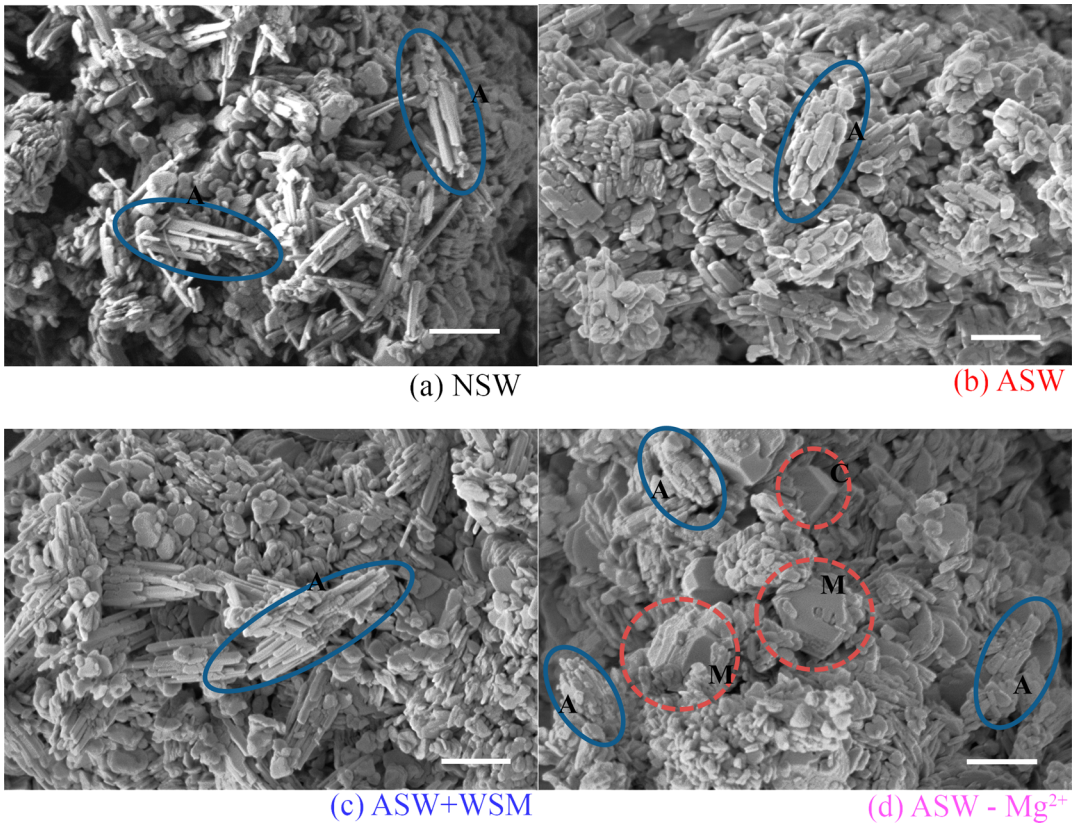

Figure 7. SEM images of precipitates obtained at the end of brucite dissolution in 900 cm^3 seawater experiments: (a) NSW; (b) ASW; (c) ASW + WSM; (d) ASW − Mg^{2+}. Scale bars are 1 μm. A = aragonite; C = calcite; M = Mg-calcite.

DOI: 10.1021/acs.cgd.6b01305
Cryst. Growth Des. 2017, 17, 1502−1513

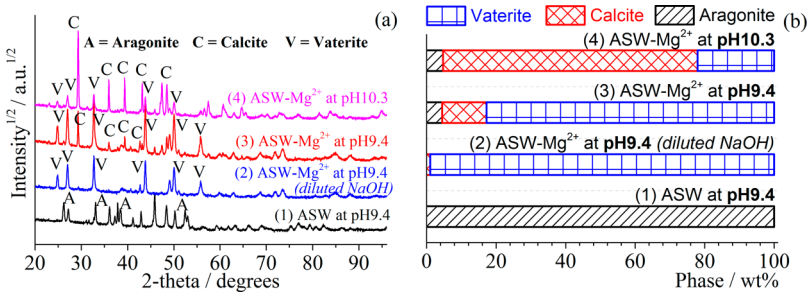

Figure 8. (a) Powder X-ray diffraction patterns and (b) $CaCO_3$ polymorph fractions of the solid powder obtained from ASW and ASW − Mg^{2+} solutions (V = 900 cm^3) at the end of NaOH addition experiments (72 h). The solution pHs are semicontrolled at 9.4 or 10.3 by adding NaOH solution.

organization (texture) of $CaCO_3$ crystals but also has some intracrystalline influence.[60] In this work, we use powders and cannot probe eventual WSM effects on crystalline organization (powders are not textured). But the morphology of the needle-like aragonite crystals in ASW + WSM (Figure 7c) become similar to those in NSW (Figure 7a), and we can then conclude this is due to the effects of *P. maxima* nacre's WSM. However, our NSW contains WSM due to dissolved bio-organisms, from many different microstructural types, not only nacres but also crossed lamellar, foliated, etc. and not from *P. maxima* (a species not present in the English Channel) but from other gastropods and bivalves (e.g., *Mytilus edulis, Pecten maximus, Crepidula fornicata*, etc.). We consequently cannot conclude that the aragonite crystal modifications are only due to nacre-like WSM content.

Although aragonite is found upon brucite dissolution in both seawaters,with or without initial Mg^{2+} ions, the aragonite crystals formed in ASW − Mg^{2+} are not similar to those precipitated in the ASW solution. This result suggests that the Mg^{2+} ions supplied by brucite dissolution (especially in ASW − Mg^{2+}) and Mg^{2+} pre-existing in the seawater have different effects on the aragonite morphology. Consequently, the aragonite morphology is affected by the Mg/Ca ratio. Calcite and Mg-calcite are also precipitated in the ASW − Mg^{2+} solution (Figure 7d). The Mg-calcite crystals formed in ASW − Mg^{2+} look like imperfect rhombs with cavities; new faces develop from the edges of "perfect" rhombohedral morphology calcite. It is important to note that abiotic precipitation of pure (Mg-free) calcite is not observed in seawater.[1] Marine calcite often contains variable amounts of Mg^{2+}, generically termed magnesian calcite. Mucci and Morse[63] suggested that larger Mg/Ca ratios in the solution result in larger incorporation of Mg^{2+} in calcite crystals, modifying crystal morphology.[64]

$CaCO_3$ Polymorphs after NaOH Addition. In this section, we study calcium carbonate polymorph precipitation in ASW with and without Mg^{2+} using NaOH addition in order to examine OH^- effects not coming from brucite dissolution. Two NaOH solutions are used: a highly concentrated (15 M) solution to avoid dilution of the solutions and changes in the ionic strength and a diluted (1 M) solution to limit strong variations in local pH. The NaOH addition allows an increase of the seawater pH to ∼9.4 or ∼10.3. These pH values were chosen to match the ones observed in seawaters after brucite dissolution. Contrarily to the brucite case, the seawater pH modification introduced by NaOH addition is not constant and decreases with time. Such a pH decrease is caused by the displacement of HCO_3^-/CO_3^{2-} equilibrium (reaction r2) and $CaCO_3$ precipitation (reaction r3). In this case, the pH of the solutions is readjusted through NaOH addition. The XRD patterns allowed quantitative determination of phase fractions in the precipitated $CaCO_3$ powders, in which the three main polymorphs, calcite, aragonite, and vaterite (by order of decreasing stability) are observed depending on the conditions (Figure 8). The morphologies of $CaCO_3$ crystals in the aggregates also vary considerably as evidenced on SEM images (Figure 9). With incorporation of NaOH, aragonite pseudohexagonal prisms are formed from the initial ASW solution (Figures 8 and 9a). These prisms, typically smaller than 300 nm in width and height, pile up along their *c*-axes to form segmented columnar particles. The aragonite crystals are not favored without Mg^{2+} addition (typical vol % lower than 5%, Figures 8 and 9b−d), to the benefit of both vaterite and calcite with the addition of NaOH. Spherical aggregates of vaterite are precipitated at pH ≈ 9.4, while imperfect rhombic calcite particles are mainly found at higher pH ≈ 10.3 from ASW without Mg^{2+} solution (Figure 9b−d). The $CaCO_3$ polymorph selection upon chemical addition then strongly depends on Mg^{2+} ions and seawater pH values. This result is consistent with the results obtained in the previous section of this study and with those reported elsewhere.[1,17] SEM images indicate that for the same testing duration (72 h), aragonite crystal sizes are larger upon NaOH addition (Figure 9a) than under brucite dissolution (Figure 7b), this latter resulting in more rounded crystals of smaller sizes. Crystals size and shape modifications are consequently the result of Mg^{2+} ions coming from brucite dissolution. Local increases in Mg^{2+} concentration close to $CaCO_3$ crystallization sites might inhibit aragonite crystal growth.

The NaOH solution addition to the ASW − Mg^{2+} solution allows both calcite and vaterite precipitation. $CaCO_3$ polymorph selection depends strongly on pH conditions, XRD (Figure 8c,d) and SEM (Figure 9c,d) indicate that calcite (∼80 wt %) is mainly precipitated when pH is controlled at a larger value of ∼10.3. Strongly metastable vaterite is also precipitated (∼20 wt %), while aragonite is only present in very small fraction in the precipitates. Morse et al.[17] found that calcite is formed in Mg-free seawater at ambient temperature. Otherwise, we find that a pH value around 9.4 leads to predominant vaterite precipitation (∼80 wt %). Moreover, only thermodynamically metastable vaterite is precipitated from ASW − Mg^{2+} when a diluted NaOH solution (1 M) is used to slowly increase pH to ∼9.4 (Figure 8b). Vaterite exhibits roughly spherical aggregates (Figure 9b) composed of many nanosized fine particles. These latter agglomerate together to form spheres in order to meet lowest energies[65] but exhibit two different internal crystal shapes and sphere mean diameter depending on the NaOH dilution (Figures 9b,c). While the use of diluted NaOH results in 4−6 μm diameter spheres with a compact arrangement (Figure 9b) of parallelepiped-like crystals, more needle-like crystals with various sizes and aspect ratio form in more porous vaterite spheres of larger 8−10 μm diameters under nondiluted NaOH 15 M addition

DOI: 10.1021/acs.cgd.6b01305
Cryst. Growth Des. 2017, 17, 1502−1513

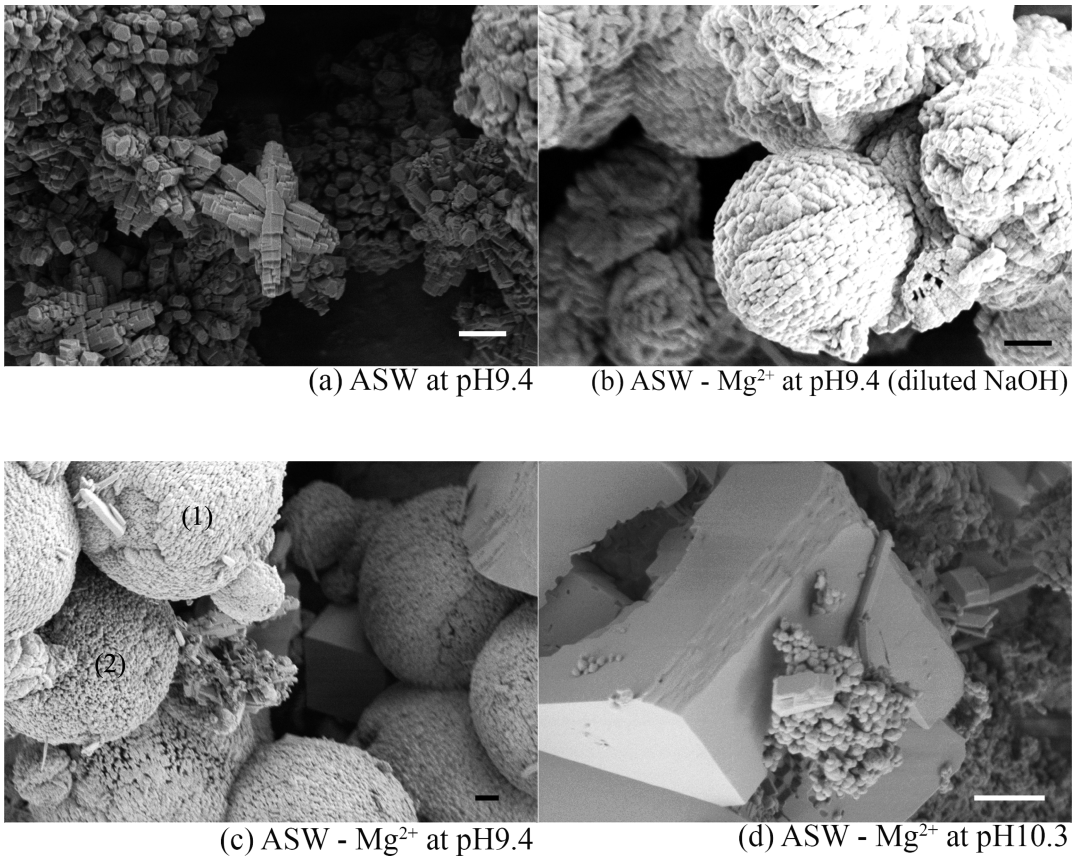

Figure 9. SEM images of precipitated powders ($CaCO_3$ polymorphs) obtained from different solutions at the end of NaOH addition experiments: (a) ASW (pH 9.4); (b) ASW − Mg^{2+} (pH 9.4) using diluted NaOH; (c) ASW − Mg^{2+} (pH 9.4); (d) ASW − Mg^{2+} (pH 10.3). Scale bars are 1 μm. (1) Tangentially and (2) radially needle-like vaterite crystals.

(Figure 9c). These needles, a few hundred nanometers in length, are variably arranged in the various vaterite spheres, for example, tangentially or radially (see the top-left (1) and middle-left (2) spheres of Figure 9b, respectively) and eventually with different orientations in the same sphere. Vaterite formation under similar conditions, that is, pH 9−10 at ambient temperature, in aqueous solutions (but not in Mg-free seawater) has already been reported.[16,65−68] While the overall sphere sizes are roughly the same, the internal crystal shapes are subjected to strong variability upon chemical inclusions during elaboration.[69−74] The vaterite crystal shapes observed in this work are not surprising thanks to this large variability and were already observed by other authors. For instance, Ouhenia et al.[75] observed vaterite spheres with longer radial needle crystals at 25 °C without Mg^{2+} ions, and some "aberrant columnar" vaterite[76] was observed in biogenic layers of the bivalve shell of *Corbicula fluminea*, in which the columns are composed of partitioned nanocrystals of vaterite as rough parallelepiped crystals. In our conditions, it is important to remind that brucite dissolution in the ASW − Mg^{2+} had led to an increase of the solution pH up to about 10.3 within the first 6 h, followed by a slow decrease down to ∼9.8. Both calcite and aragonite but not vaterite polymorphs were found in the precipitate upon brucite dissolution. These results suggest that pH plays a major role in the vaterite phase selection from Mg-free seawater, pH values not larger than typically 9.4 allowing vaterite precipitation while larger pH values favor predominantly calcite under such conditions. Our results are consistent with those of Sheng Han et al.[65] who found that vaterite was mainly formed at low pH, while both vaterite and some rhombic calcite particles crystallized at larger pH. Hu et al.[77] also found that vaterite was precipitated from $CaCl_2$ and $NaHCO_3$ mixtures at near-freezing temperature and moderate alkaline conditions (pH 9.0). However, another parameter governing the $CaCO_3$ phase selection is the presence of Mg^{2+} ions. Mg^{2+} ions in ASW have inhibited vaterite and calcite formation. Thus, results obtained in this section upon NaOH addition are coherent with former results indicating brucite dissolution in the seawaters favored aragonite precipitation by both pH increase and presence of Mg^{2+} ions. If the effect of Mg^{2+} ions has already been related as calcite growth inhibitor, the presence of Mg^{2+} ions provided from brucite dissolution (even keeping a low Mg/Ca ratio) in this study also prompts for the vaterite inhibition potential.

■ CONCLUSIONS

Brucite ($Mg(OH)_2$) dissolution in seawaters leads to favorable conditions for $CaCO_3$ precipitation. $CaCO_3$ polymorphs and morphologies are controlled by pH and magnesium concentration. On one hand, the predominance of vaterite or calcite precipitated from Mg-free seawaters can be adjusted under pH-controlled conditions by NaOH addition. On the other hand, addition of Mg^{2+} ions in seawater or working with natural seawater inhibits calcite and vaterite growth and precipitation and favors aragonite occurrence. Consequently, it is demonstrated in this work that brucite dissolution in seawaters provides both the necessary Mg^{2+} ions and the pH increase necessary to stabilize aragonite precipitation under ambient conditions. WSM addition has no or minor effect on the aragonite cell parameters but

DOI: 10.1021/acs.cgd.6b01305
Cryst. Growth Des. 2017, 17, 1502−1513

modifies their crystal shapes. Aragonite crystals obtained from ASW + WSM and from NSW have similar morphology.

■ ASSOCIATED CONTENT

Supporting Information

The Supporting Information is available free of charge on the ACS Publications website at DOI: 10.1021/acs.cgd.6b01305.

PHREEQC model outcome showing the evolution of pH and SI values of relevant phases as a function of dissolved brucite at 20 °C and pH and saturation indices for aragonite, calcite, dolomite, magnesite, and monohydrocalcite calculated at brucite equilibrium in different solutions at 20 °C (PDF)

■ AUTHOR INFORMATION

Corresponding Author

*D.N.D. E-mail addresses: dang-dan.nguyen@unicaen.fr, ddan.nguyen@gmail.com.

ORCID

Dan Nguyen Dang: 0000-0003-1334-8914

Author Contributions

The manuscript was written through contributions of all authors. All authors have given approval to the final version of the manuscript.

Funding

Financial support for this research was provided by the French National Research Agency (ANR-13-RMNP-0004) and by the Conseil Régional de Normandie, France.

Notes

The authors declare no competing financial interest.

■ ACKNOWLEDGMENTS

We are grateful to three anonymous referees for their careful reviews and valuable comments that helped us to improve the quality of this manuscript.

■ ABBREVIATIONS

NSW, natural seawater; ASW, artificial seawater; WSM, water-soluble organic matrix extracted from the nacre of oyster *Pinctada margaritifera*; ASW + WSM, artificial seawater with WSM added; ASW − Mg^{2+}, artificial seawater without magnesium ions

■ REFERENCES

(1) Morse, J. W.; Arvidson, R. S.; Lüttge, A. Calcium Carbonate Formation and Dissolution. *Chem. Rev.* **2007**, *107*, 342−381.

(2) Addadi, L.; Raz, S.; Weiner, S. Taking Advantage of Disorder: Amorphous Calcium Carbonate and Its Roles in Biomineralization. *Adv. Mater.* **2003**, *15*, 959−970.

(3) Rieger, J.; Frechen, T.; Cox, G.; Heckmann, W.; Schmidt, C.; Thieme, J. Precursor structures in the crystallization/precipitation processes of CaCO3 and control of particle formation by polyelectrolytes. *Faraday Discuss.* **2007**, *136*, 265−277.

(4) Gebauer, D.; Völkel, A.; Cölfen, H. Stable Prenucleation Calcium Carbonate Clusters. *Science* **2008**, *322*, 1819−1822.

(5) Tribello, G. A.; Bruneval, F.; Liew, C.; Parrinello, M. A Molecular Dynamics Study of the Early Stages of Calcium Carbonate Growth. *J. Phys. Chem. B* **2009**, *113*, 11680−11687.

(6) Sarkar, A.; Mahapatra, S. Synthesis of All Crystalline Phases of Anhydrous Calcium Carbonate. *Cryst. Growth Des.* **2010**, *10*, 2129−2135.

(7) Sand, K. K.; Rodriguez-Blanco, J. D.; Makovicky, E.; Benning, L. G.; Stipp, S. L. S. Crystallization of CaCO3 in Water−Alcohol Mixtures: Spherulitic Growth, Polymorph Stabilization, and Morphology Change. *Cryst. Growth Des.* **2012**, *12*, 842−853.

(8) Kabalah-Amitai, L.; Mayzel, B.; Kauffmann, Y.; Fitch, A. N.; Bloch, L.; Gilbert, P. U. P. A.; Pokroy, B. Vaterite Crystals Contain Two Interspersed Crystal Structures. *Science* **2013**, *340*, 454−457.

(9) Koga, N.; Kasahara, D.; Kimura, T. Aragonite Crystal Growth and Solid-State Aragonite−Calcite Transformation: A Physico−Geometrical Relationship via Thermal Dehydration of Included Water. *Cryst. Growth Des.* **2013**, *13*, 2238−2246.

(10) Nishiyama, R.; Munemoto, T.; Fukushi, K. Formation condition of monohydrocalcite from CaCl2−MgCl2−Na2CO3 solutions. *Geochim. Cosmochim. Acta* **2013**, *100*, 217−231.

(11) Sarkar, A.; Dutta, K.; Mahapatra, S. Polymorph Control of Calcium Carbonate Using Insoluble Layered Double Hydroxide. *Cryst. Growth Des.* **2013**, *13*, 204−211.

(12) Wang, H.; Alfredsson, V.; Tropsch, J.; Ettl, R.; Nylander, T. Formation of CaCO3 Deposits on Hard Surfaces—Effect of Bulk Solution Conditions and Surface Properties. *ACS Appl. Mater. Interfaces* **2013**, *5*, 4035−4045.

(13) WILBUR, K. M.; BERNHARDT, A. M. Effects of amino acids, magnesium, and molluscan extrapallial fluid on crystallization of calcium carbonate: in vitro experiments. *Biol. Bull.* **1984**, *166*, 251−259.

(14) Mucci, A.; Canuel, R.; Zhong, S. The solubility of calcite and aragonite in sulfate-free seawater and the seeded growth kinetics and composition of the precipitates at 25°C. *Chem. Geol.* **1989**, *74*, 309−320.

(15) Zhong, S.; Mucci, A. Calcite and aragonite precipitation from seawater solutions of various salinities: Precipitation rates and overgrowth compositions. *Chem. Geol.* **1989**, *78*, 283−299.

(16) Verdoes, D.; Kashchiev, D.; van Rosmalen, G. M. Determination of nucleation and growth rates from induction times in seeded and unseeded precipitation of calcium carbonate. *J. Cryst. Growth* **1992**, *118*, 401−413.

(17) Morse, J. W.; Wang, Q.; Tsio, M. Y. Influences of temperature and Mg:Ca ratio on CaCO3 precipitates from seawater. *Geology* **1997**, *25*, 85−87.

(18) Zuddas, P.; Mucci, A. Kinetics of Calcite Precipitation from Seawater: II. The Influence of the Ionic Strength. *Geochim. Cosmochim. Acta* **1998**, *62*, 757−766.

(19) De Choudens-Sánchez, V.; González, L. A. Calcite and Aragonite Precipitation Under Controlled Instantaneous Supersaturation: Elucidating the Role of CaCO3 Saturation State and Mg/Ca Ratio on Calcium Carbonate Polymorphism. *J. Sediment. Res.* **2009**, *79*, 363−376.

(20) Falini, G.; Fermani, S.; Tosi, G.; Dinelli, E. Calcium Carbonate Morphology and Structure in the Presence of Seawater Ions and Humic Acids. *Cryst. Growth Des.* **2009**, *9*, 2065−2072.

(21) Sun, W.; Jayaraman, S.; Chen, W.; Persson, K. A.; Ceder, G. Nucleation of metastable aragonite CaCO3 in seawater. *Proc. Natl. Acad. Sci. U. S. A.* **2015**, *112*, 3199−3204.

(22) Tas, A. C. Aragonite coating solutions (ACS) based on artificial seawater. *Appl. Surf. Sci.* **2015**, *330*, 262−269.

(23) Neumann, M.; Epple, M. Monohydrocalcite and Its Relationship to Hydrated Amorphous Calcium Carbonate in Biominerals. *Eur. J. Inorg. Chem.* **2007**, *2007*, 1953−1957.

(24) Cölfen, H.; Mann, S. Higher-Order Organization by Mesoscale Self-Assembly and Transformation of Hybrid Nanostructures. *Angew. Chem., Int. Ed.* **2003**, *42*, 2350−2365.

(25) Berner, R. A.; Westrich, J. T.; Graber, R.; Smith, J.; Martens, C. S. Inhibition of aragonite precipitation from supersaturated seawater; a laboratory and field study. *Am. J. Sci.* **1978**, *278*, 816−837.

(26) Berner, R. A. The role of magnesium in the crystal growth of calcite and aragonite from sea water. *Geochim. Cosmochim. Acta* **1975**, *39*, 489−504.

(27) Davis, K. J.; Dove, P. M.; De Yoreo, J. J. The Role of Mg2+ as an Impurity in Calcite Growth. *Science* **2000**, *290*, 1134−1137.

(28) Cusack, M.; Freer, A. Biomineralization: Elemental and Organic Influence in Carbonate Systems. *Chem. Rev.* **2008**, *108*, 4433−4454.

(29) Marin, F.; Luquet, G.; Marie, B.; Medakovic, D. Molluscan Shell Proteins: Primary Structure, Origin, and Evolution. In *Current Topics in*

DOI: 10.1021/acs.cgd.6b01305
Cryst. Growth Des. 2017, 17, 1502−1513

Developmental Biology; Schatten, G., Ed.; Academic Press: Boston, MA, 2007; Vol. *80*, pp 209−276.
(30) Rousseau, M.; Pereira-Mouriès, L.; Almeida, M.-J.; Milet, C.; Lopez, E. The water-soluble matrix fraction from the nacre of Pinctada maxima produces earlier mineralization of MC3T3-E1 mouse pre-osteoblasts. *Comp. Biochem. Physiol., Part B: Biochem. Mol. Biol.* **2003**, *135*, 1−7.
(31) Atlan, G.; Delattre, O.; Berland, S.; LeFaou, A.; Nabias, G.; Cot, D.; Lopez, E. Interface between bone and nacre implants in sheep. *Biomaterials* **1999**, *20*, 1017−1022.
(32) Lamghari, M.; Almeida, M. J.; Berland, S.; Huet, H.; Laurent, A.; Milet, C.; Lopez, E. Stimulation of bone marrow cells and bone formation by nacre: in vivo and in vitro studies. *Bone* **1999**, *25*, 91S−94S.
(33) Lopez, E.; Faou, A. L.; Borzeix, S.; Berland, S. Stimulation of rat cutaneous fibroblasts and their synthetic activity by implants of powdered nacre (mother of pearl). *Tissue Cell* **2000**, *32*, 95−101.
(34) Atlan, G.; Balmain, N.; Berland, S.; Vidal, B.; Lopez, É. Reconstruction of human maxillary defects with nacre powder: histological evidence for bone regeneration. *C. R. Acad. Sci., Ser. III* **1997**, *320*, 253−258.
(35) Estrada, C. F.; Sverjensky, D. A.; Pelletier, M.; Razafitianamaharavo, A.; Hazen, R. M. Interaction between l-aspartate and the brucite [Mg(OH)2]−water interface. *Geochim. Cosmochim. Acta* **2015**, *155*, 172−186.
(36) Kelley, D. S.; Karson, J. A.; Früh-Green, G. L.; Yoerger, D. R.; Shank, T. M.; Butterfield, D. A.; Hayes, J. M.; Schrenk, M. O.; Olson, E. J.; Proskurowski, G.; Jakuba, M.; Bradley, A.; Larson, B.; Ludwig, K.; Glickson, D.; Buckman, K.; Bradley, A. S.; Brazelton, W. J.; Roe, K.; Elend, M. J.; Delacour, A.; Bernasconi, S. M.; Lilley, M. D.; Baross, J. A.; Summons, R. E.; Sylva, S. P. A Serpentinite-Hosted Ecosystem: The Lost City Hydrothermal Field. *Science* **2005**, *307*, 1428−1434.
(37) Ohara, Y.; Reagan, M. K.; Fujikura, K.; Watanabe, H.; Michibayashi, K.; Ishii, T.; Stern, R. J.; Pujana, I.; Martinez, F.; Girard, G.; Ribeiro, J.; Brounce, M.; Komori, N.; Kino, M. A serpentinite-hosted ecosystem in the Southern Mariana Forearc. *Proc. Natl. Acad. Sci. U. S. A.* **2012**, *109*, 2831−2835.
(38) Vermilyea, D. A. The Dissolution of MgO and Mg (OH) 2 in Aqueous Solutions. *J. Electrochem. Soc.* **1969**, *116*, 1179−1183.
(39) Jordan, G.; Rammensee, W. Dissolution rates and activation energy for dissolution of brucite (001): A new method based on the microtopography of crystal surfaces. *Geochim. Cosmochim. Acta* **1996**, *60*, 5055−5062.
(40) Pokrovsky, O. S.; Schott, J. Experimental study of brucite dissolution and precipitation in aqueous solutions: surface speciation and chemical affinity control. *Geochim. Cosmochim. Acta* **2004**, *68*, 31−45.
(41) Pokrovsky, O. S.; Schott, J.; Castillo, A. Kinetics of brucite dissolution at 25°C in the presence of organic and inorganic ligands and divalent metals. *Geochim. Cosmochim. Acta* **2005**, *69*, 905−918.
(42) Neville, A.; Morizot, A. P. Calcareous scales formed by cathodic protection—an assessment of characteristics and kinetics. *J. Cryst. Growth* **2002**, *243*, 490−502.
(43) Barchiche, C.; Deslouis, C.; Festy, D.; Gil, O.; Refait, P.; Touzain, S.; Tribollet, B. Characterization of calcareous deposits in artificial seawater by impedance techniques: 3—Deposit of CaCO3 in the presence of Mg(II). *Electrochim. Acta* **2003**, *48*, 1645−1654.
(44) Barchiche, C.; Deslouis, C.; Gil, O.; Joiret, S.; Refait, P.; Tribollet, B. Role of sulphate ions on the formation of calcareous deposits on steel in artificial seawater; the formation of Green Rust compounds during cathodic protection. *Electrochim. Acta* **2009**, *54*, 3580−3588.
(45) ASTM D1141-98(2013), Standard Practice for the Preparation of Substitute Ocean Water; ASTM International, West Conshohocken, PA, 2013.
(46) Rousseau, M.; Plouguerné, E.; Wan, G.; Wan, R.; Lopez, E.; Fouchereau-Peron, M. Biomineralisation markers during a phase of active growth in Pinctada margaritifera. *Comp. Biochem. Physiol., Part A: Mol. Integr. Physiol.* **2003**, *135*, 271−278.
(47) Bédouet, L.; Rusconi, F.; Rousseau, M.; Duplat, D.; Marie, A.; Dubost, L.; Le Ny, K.; Berland, S.; Péduzzi, J.; Lopez, E. Identification of low molecular weight molecules as new components of the nacre organic matrix. *Comp. Biochem. Physiol., Part B: Biochem. Mol. Biol.* **2006**, *144*, 532−543.
(48) Parkhurst, D. L.; Appelo, C. A. J. Description of input and examples for PHREEQC version 3—A computer program for speciation, batch-reaction, one-dimensional transport, and inverse geochemical calculations; U.S. Geological Survey Techniques and Methods; 2013; book 6, chap. A43, 497 pp.
(49) Chateigner, D. *Combined Analysis*; John Wiley & Sons, Inc.: Hoboken, NJ, USA, 2010.
(50) Dreybrodt, W.; Eisenlohr, L.; Madry, B.; Ringer, S. Precipitation kinetics of calcite in the system CaCO3 H2O C02: The conversion to CO2 by the slow process H++HCO3− → CO2+H2O as a rate limiting step. *Geochim. Cosmochim. Acta* **1997**, *61*, 3897−3904.
(51) Ciftja, A. F.; Hartono, A.; Svendsen, H. F. Selection of Amine Amino Acids Salt Systems for CO2 Capture. *Energy Procedia* **2013**, *37*, 1597−1604.
(52) Suess, E. Interaction of organic compounds with calcium carbonate-II. Organo-carbonate association in Recent sediments. *Geochim. Cosmochim. Acta* **1973**, *37*, 2435−2447.
(53) Sayles, F. L.; Fyfe, W. S. The crystallization of magnesite from aqueous solution. *Geochim. Cosmochim. Acta* **1973**, *37*, 87−99.
(54) Hövelmann, J.; Putnis, C. V.; Ruiz-Agudo, E.; Austrheim, H. Direct Nanoscale Observations of CO2 Sequestration during Brucite [Mg(OH)2] Dissolution. *Environ. Sci. Technol.* **2012**, *46*, 5253−5260.
(55) Radha, A. V.; Navrotsky, A. Thermodynamics of Carbonates. *Rev. Mineral. Geochem.* **2013**, *77*, 73−121.
(56) Lutterotti, L.; Matthies, S.; Wenk, H. MAUD: a friendly Java program for material analysis using diffraction. *Newsletter of the CPD* **1999**, *21*, 14−15.
(57) Nielsen, M. R.; Sand, K. K.; Rodriguez-Blanco, J. D.; Bovet, N.; Generosi, J.; Dalby, K. N.; Stipp, S. L. S. Inhibition of Calcite Growth: Combined Effects of Mg2+ and SO42−. *Cryst. Growth Des.* **2016**, *16*, 6199−6207.
(58) Munemoto, T.; Fukushi, K. Transformation kinetics of monohydrocalcite to aragonite in aqueous solutions. *J. Mineral. Petrol. Sci.* **2008**, *103*, 345−349.
(59) Caspi, E.; Pokroy, B.; Lee, P.; Quintana, J.; Zolotoyabko, E. On the structure of aragonite. *Acta Crystallogr., Sect. B: Struct. Sci.* **2005**, *61*, 129−132.
(60) Chateigner, D.; Ouhenia, S.; Krauss, C.; Belkhir, M.; Morales, M. Structural distortion of biogenic aragonite in strongly textured mollusc shell layers. *Nucl. Instrum. Methods Phys. Res., Sect. B* **2010**, *268*, 341−345.
(61) Chateigner, D.; Ouhenia, S.; Krauss, C.; Hedegaard, C.; Gil, O.; Morales, M.; Lutterotti, L.; Rousseau, M.; Lopez, E. Voyaging around nacre with the X-ray shuttle: From bio-mineralisation to prosthetics via mollusc phylogeny. *Mater. Sci. Eng., A* **2010**, *528*, 37−51.
(62) Krauss, C. Couches polycristallines orientées d'aragonite biomimétique, synthétisées par voie électrochimique. Ph.D. thesis, Normandie Univ, ENSICAEN, UNICAEN, CNRS, CRISMAT, 2009.
(63) Mucci, A.; Morse, J. W. The incorporation of Mg2+ and Sr2+ into calcite overgrowths: influences of growth rate and solution composition. *Geochim. Cosmochim. Acta* **1983**, *47*, 217−233.
(64) Zhang, Y.; Dawe, R. A. Influence of Mg2+ on the kinetics of calcite precipitation and calcite crystal morphology. *Chem. Geol.* **2000**, *163*, 129−138.
(65) Sheng Han, Y.; Hadiko, G.; Fuji, M.; Takahashi, M. Crystallization and transformation of vaterite at controlled pH. *J. Cryst. Growth* **2006**, *289*, 269−274.
(66) Gómez-Morales, J.; Torrent-Burgués, J.; Rodríguez-Clemente, R. Nucleation of calcium carbonate at different initial pH conditions. *J. Cryst. Growth* **1996**, *169*, 331−338.
(67) Xyla, A. G.; Giannimaras, E. K.; Koutsoukos, P. G. A collection of Papers Presented at the Symposium on Colloids in Environmental and Materials Technologies held during the 62nd ACS Colloids and Surface ScienceThe precipitation of calcium carbonate in aqueous solutions. *Colloids Surf.* **1991**, *53*, 241−255.

DOI: 10.1021/acs.cgd.6b01305
Cryst. Growth Des. 2017, 17, 1502−1513

(68) Spanos, N.; Koutsoukos, P. G. Kinetics of Precipitation of Calcium Carbonate in Alkaline pH at Constant Supersaturation. Spontaneous and Seeded Growth. *J. Phys. Chem. B* **1998**, *102*, 6679−6684.
(69) Liu, X.; Zhang, L.; Wang, Y.; Guo, C.; Wang, E. Biomimetic Crystallization of Unusual Macroporous Calcium Carbonate Spherules in the Presence of Phosphatidylglycerol Vesicles. *Cryst. Growth Des.* **2008**, *8*, 759−762.
(70) Wei, H.; Shen, Q.; Zhao, Y.; Wang, D.; Xu, D. Crystallization habit of calcium carbonate in the presence of sodium dodecyl sulfate and/or polypyrrolidone. *J. Cryst. Growth* **2004**, *260*, 511−516.
(71) Pai, R. K.; Jansson, K.; Hedin, N. Transport-Mediated Control of Particles of Calcium Carbonate. *Cryst. Growth Des.* **2009**, *9*, 4581−4583.
(72) Mihai, M.; Damaceanu, M.-D.; Aflori, M.; Schwarz, S. Calcium Carbonate Microparticles Growth Templated by an Oxadiazole-Functionalized Maleic Anhydride-co-N-vinyl-pyrrolidone Copolymer, with Enhanced pH Stability and Variable Loading Capabilities. *Cryst. Growth Des.* **2012**, *12*, 4479−4486.
(73) Geng, X.; Liu, L.; Jiang, J.; Yu, S.-H. Crystallization of CaCO3 Mesocrystals and Complex Aggregates in a Mixed Solvent Media Using Polystyrene Sulfonate as a Crystal Growth Modifier. *Cryst. Growth Des.* **2010**, *10*, 3448−3453.
(74) Dupont, L.; Portemer, F.; Figlarz, M. Synthesis and study of a well crystallized CaCO3 vaterite showing a new habitus. *J. Mater. Chem.* **1997**, *7*, 797−800.
(75) Ouhenia, S.; Chateigner, D.; Belkhir, M. A.; Guilmeau, E.; Krauss, C. Synthesis of calcium carbonate polymorphs in the presence of polyacrylic acid. *J. Cryst. Growth* **2008**, *310*, 2832−2841.
(76) Frenzel, M.; Harrison, R. J.; Harper, E. M. Nanostructure and crystallography of aberrant columnar vaterite in Corbicula fluminea (Mollusca). *J. Struct. Biol.* **2012**, *178*, 8−18.
(77) Hu, Y.-B.; Wolthers, M.; Wolf-Gladrow, D. A.; Nehrke, G. Effect of pH and Phosphate on Calcium Carbonate Polymorphs Precipitated at near-Freezing Temperature. *Cryst. Growth Des.* **2015**, *15*, 1596−1601.

DOI: 10.1021/acs.cgd.6b01305
Cryst. Growth Des. 2017, 17, 1502−1513